

6

***In Vivo* Cell Biology of Cancer Cells Visualized with Fluorescent Proteins**

Robert M. Hoffman

AntiCancer, Inc.

San Diego, California 92111

- I. Introduction
 - II. Whole-Body Imaging of Tumor Growth and Metastasis
 - III. Whole-Body and Intravital Imaging of Angiogenesis and Individual Tumor Cells
 - IV. Dual-Color Imaging
 - V. Dual-Color Tumor–Host Models
 - VI. Intravital Imaging of GFP-Expressing Cells
 - VII. Imaging GFP Tumor Cells in Blood Vessels
 - VIII. Clinically Applicable Models of GFP Tumor Imaging
 - IX. Fluorescent Reporter Gene for Human T Cells
 - X. Bone Marrow Protection by Transfer of Drug-Resistance Genes Coupled to GFP
 - XI. Molecular Imaging
 - XII. Chemotherapy Effects of a Senescence Program Controlled by p53 and p16^{INK4a}
 - XIII. Conclusions and Future Directions
- Acknowledgments
References

This chapter describes a new cell biology where the behavior of individual cells can be visualized in the living animal. Previously it has been demonstrated that fluorescent proteins can be used for whole-body imaging of metastatic tumor growth, bacterial infection, and gene expression. An example of the new cell biology is dual-color fluorescence imaging using red fluorescent protein (RFP)-expressing tumors transplanted in green fluorescent protein (GFP)-expressing transgenic mice. These models show with great clarity the details of tumor–stroma interactions and especially tumor-induced angiogenesis, tumor-infiltrating lymphocytes, stromal fibroblasts, and macrophages. Another example is the color coding of cells with RFP or GFP such that both cell types can be simultaneously visualized *in vivo*. Stem cells can also be visualized and tracked *in vivo*. Mice in which the regulatory elements of the stem cell marker nestin drive GFP expression enable nascent vasculature to be visualized interacting with transplanted RFP-expressing cancer cells. Nestin-driven GFP expression can also be used to visualize hair follicle stem cells. Dual-color cells expressing GFP in the nucleus and RFP in the cytoplasm enable real-time visualization of nuclear–cytoplasm dynamics including cell cycle events and apoptosis. Highly elongated cancer

cells in capillaries in living mice were observed within skin flaps. The migration velocities of the cancer cells in the capillaries were measured by capturing images of the dual-color fluorescent cells over time. The cells in the capillaries elongated to fit the width of these vessels. The use of the dual-color cancer cells differentially labeled in the cytoplasm and nucleus and associated fluorescent imaging provide a powerful tool to understand the mechanism of cancer cell migration and deformation in small vessels. © 2005, Elsevier Inc.

I. Introduction

Animal models of cancer that use the stable expression of green fluorescent protein (GFP) and red fluorescent protein (RFP) have made it possible to directly observe cell behavior in live animals. The interaction of cells with each other and entry of tumor cells into the circulation are important factors in metastasis. These processes can be observed using fluorescent proteins in real time (Yamauchi *et al.*, 2005). Before the introduction of GFP, intravital imaging was limited to the study of cells that were transiently labeled with vital dyes.

Initial studies of tumor biology that used stable GFP expression focused on static images and examination of metastases. The first use of stable GFP expression to characterize cancer cells *in vivo* was by Chishima *et al.* (1997a). Cell motility, shape changes, and migration of carcinoma cells expressing GFP in live animals *in vivo* was first described by Farina *et al.* (1998). Huang *et al.* (2002) demonstrated that GFP-transduced H1299 lung cancer cells allowed the imaging of local invasion at the single-cell level. Tumor cells in blood vessels were readily imaged. Wyckoff *et al.* (2000) have measured tumor cell density in the blood using intravital GFP imaging. Wyckoff *et al.* (2000) have used GFP imaging to view cells in time-lapse images within a single optical section using a confocal microscope. Naumov *et al.* (1999) visualized CHO-K1 cells that stably express GFP. Fine cellular details such as pseudopodial projections, even after extended periods of *in vivo* growth, were visualized by GFP expression. Mook *et al.* (2003) generated a GFP-expressing rat adenocarcinoma cell line (CC531s) that forms metastases in rat liver after administration to the portal vein. Initial arrest of colon cancer cells in sinusoids of the liver was due to size restriction. Tumor cells divided exclusively intravascularly during the first 4 days. We visualized the trafficking of metastatic cells targeting the liver via the portal vein using GFP-expressing cancer cells. Within 72 hours after transplantation on the ascending colon in nude mice, metastasis was visualized *ex vivo* on a single-cell basis around the portal vein by GFP imaging (Wang *et al.*, 2004). Al-Mehdi *et al.* (2000) observed the steps in early hematogenous metastasis of tumor

cells expressing GFP in subpleural microvessels in intact, perfused mouse and rat lungs. Metastatic tumor cells attached to the endothelia of pulmonary precapillary arterioles and capillaries. Extravasation of tumor cells was rare. Early tumor colonies were observed entirely within the blood vessels. Brown *et al.* (2001) showed that multiphoton laser-scanning microscopy could provide high-resolution three-dimensional images of angiogenesis gene expression and that this technique could be used to investigate deeper regions of GFP-expressing tumors in dorsal skinfold chambers. To monitor the activity of the vascular endothelial growth factor (VEGF) promoter, Fukumura *et al.* (1997, 1998) made transgenic mice that express GFP under control of the VEGF promoter. Multiphoton laser scanning microscopy showed that the tumor was able to induce activity of the VEGF promoter; GFP-positive stromal cells were seen at least 200 μm into the tumor with this technique.

Yamamoto *et al.* (2004) reported the genetic engineering of dual-color fluorescent cells with one color in the nucleus and the other in the cytoplasm that allows real-time nuclear-cytoplasmic dynamics to be visualized in living cells *in vivo* as well as *in vitro*. To obtain the dual-color cells, RFP was expressed in the cytoplasm of HT1080 human fibrosarcoma cells, and GFP linked to histone H2B was expressed in the nucleus. Nuclear GFP expression enabled visualization of nuclear dynamics, whereas simultaneous cytoplasmic RFP expression enabled visualization of nuclear-cytoplasmic ratios as well as simultaneous cell and nuclear shape changes. Thus, total cellular dynamics can be visualized in the dual-color cells in real time (Fig. 1). Common carotid artery injection of dual-color cells and a reversible skin flap enabled the external visualization of the dual-color cells in microvessels in the mouse brain where extreme elongation of the cell body as well as the nucleus occurred.

II. Whole-Body Imaging of Tumor Growth and Metastasis

The use of fluorescent proteins for both whole-body and intravital cellular imaging is reviewed in the following text. External whole-body imaging of mice with primary and metastatic tumors that are genetically labeled with the fluorescent proteins GFP and RFP is a simple but powerful tool for investigating tumor development. The technology is based on the bright intrinsic fluorescence of GFP and RFP, which is partly caused by the high quantum yield of these fluorophores (Heim *et al.*, 1995; Matz *et al.*, 1999). For tumor cells to be visualized with this technique, they must be transduced with GFP or RFP genes so that they become brightly fluorescent. This can be accomplished by *in vitro* (Chishima *et al.*, 1997b; Yang *et al.*, 2000) and *in vivo* (Hasegawa *et al.*, 2000) selection of such fluorescent tumor cells.

To produce metastasis in mice, the genetically fluorescent tumors should be transplanted orthotopically (Bouvet *et al.*, 2000, 2002; Chishima *et al.*,

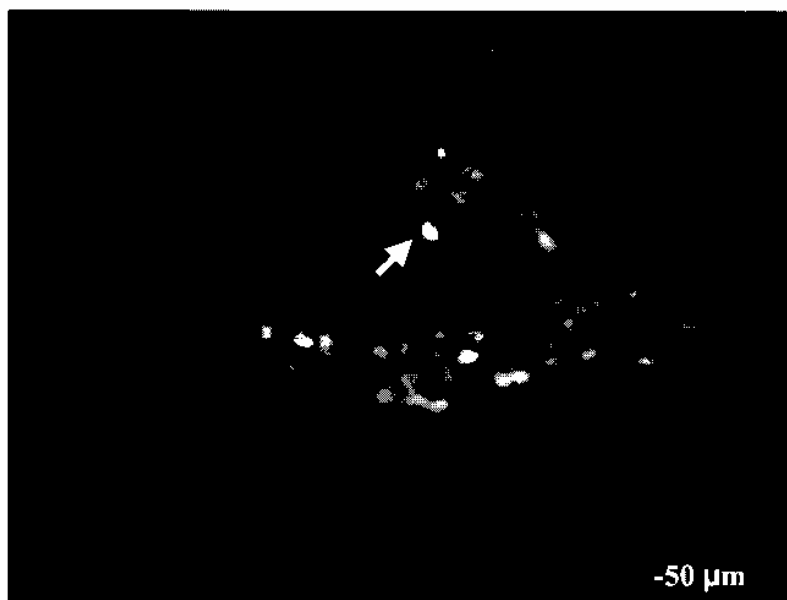


Figure 1 Extravasation of tumor cells from vessels containing numerous dual-color HT1080 fibrosarcoma cells in a living mouse. HT1080 human fibrosarcoma cells were labeled with histone-H2B-GFP in the nucleus and with retroviral RFP in the cytoplasm. Cells were injected in the heart and visualized in skin vessels by whole-body imaging. From K. Yamauchi and R. M. Hoffman, unpublished data. (See Color Insert.)

1997b,c; Hastings *et al.*, 2001; Maeda *et al.*, 2000; Rashidi *et al.*, 2000; Yang *et al.*, 1998, 1999a,b, 2001).

Once the GFP-expressing tumors have developed and metastases have formed, individual tumor cells can be detected in the live mouse by use of whole-body imaging with fairly simple equipment. A fluorescence light box with fiberoptic lighting at ~490 nm and appropriate filters, placed on top of the light box, can be used to image large tumors and can be viewed with the naked eye (Yang *et al.*, 2000). Alternatively, the light box can be linked to a camera with an appropriate filter to enable images to be displayed on a monitor and digitally stored (Yang *et al.*, 2000). To visualize smaller tumors and metastases, the animal can be put on a fluorescence dissecting microscope that incorporates a light source and filters for excitation at ~490 nm. Fluorescence emission can be observed through a 520 nm long-pass filter (Yang *et al.*, 2000). The animals can be irradiated at 490 nm for long periods without harming them or bleaching the GFP or RFP fluorescence. Images can be processed with standard software and the imaging procedures can be repeated as often as necessary without harming the animal. Therefore, with these techniques real-time tracking of tumor growth and metastasis is feasible.

Reversible skin flaps can also be introduced onto different parts of the animal to examine single tumor cells or small colonies on internal organs (Yang *et al.*, 2002). The skin flaps are rendered reversible by simple suturing.

External imaging can then be done through the relatively transparent body walls of the mouse, which include the skull, by use of a fluorescence dissecting microscope. Blood vessels growing on tumors can also be observed using skin flaps because they contrast with the fluorescence of the tumors (Yang *et al.*, 2002). Examples of findings from studies of these techniques are described below.

Transplanted mice with metastatic lesions of GFP-expressing tumors in the colon, brain, liver, lymph nodes, and bone have been used to produce images of metastasis. These images are used for real-time quantitative measurement of primary and metastatic tumor growth for each of these organs. GFP-expressing cells emit a bright fluorescence signal compared with background fluorescence from other tissue. The signal is so strong and selective that external images of GFP-expressing tumors and their metastases can be obtained in freely moving animals (Yang *et al.*, 2000).

In another study, an RFP-expressing human pancreatic tumor cell line was introduced as tissue fragments into the pancreases of nude mice by surgical orthotopic implantation. As the tumors were growing, whole-body optical imaging was used to track, in real time, the growth of the primary tumor and the formation of metastatic lesions that developed in the spleen, bowel, portal lymph nodes, omentum, and liver. The images were used for quantification of tumor growth in each of these organs (Katz *et al.*, 2003a). Whole-body imaging with this model was used to compare standard and experimental agents for pancreatic cancer (Katz *et al.*, 2003b, 2004).

Peyruchaud *et al.* (2001) established a GFP-expressing bone-metastasis subclone of MDA-MB-231 (B02/GFP.2) by repeated *in vivo* passages in bone, by use of the heart injection model. When injected into the tail vein of mice, the selected cells grew preferentially in bone. Whole-body fluorescence imaging of the live mice showed that bone metastases could be detected about 1 week before radiologically distinctive osteolytic lesions developed. Furthermore, when the tumor-bearing mice were treated with a bisphosphonate, progression of established osteolytic lesions, and the expansion of breast cancer cells within bone, were inhibited.

The MDA-MB-435 human breast carcinoma cell line produced widespread osteolytic skeletal metastases following injection into the left ventricle of the heart. Osseous metastases localized predominantly to trabecular regions, especially proximal and distal femur, proximal tibia, proximal humerus, and lumbar vertebrae. GFP permitted detection of single cells and microscopic metastases in bone at early time points (Harms and Welch, 2003).

Using a different approach, human ovarian tumor cells (SKOV3.ip1) were made to express GFP by infection with a replication-deficient adenoviral (Ad) vector encoding GFP (Chaudhuri *et al.*, 2001). The infected cells showed high GFP fluorescence, and when implanted into mice, intraperitoneal tumors as small as 0.2 mm in diameter could be detected by whole-body imaging within

24 hours (Chaudhuri *et al.*, 2003). In another study, however, GFP-expressing tumors could not be detected by whole-body imaging until 7 days after subcutaneous tumor cell inoculation (Choy *et al.*, 2003). These results strongly contrast with the results described previously. This discrepancy shows the need to use appropriate instrumentation and techniques for whole-body imaging.

III. Whole-Body and Intravital Imaging of Angiogenesis and Individual Tumor Cells

Tumor angiogenesis can also be visualized by use of GFP techniques. The footpads of mice are quite transparent with few resident blood vessels and are therefore ideal for quantitative imaging of tumor angiogenesis in intact animals. Vessels can be seen because of their striking contrast to the GFP fluorescence of the tumor tissue (Yang *et al.*, 2001). These researchers injected GFP-expressing Lewis lung carcinoma cells subcutaneously into the footpad of nude mice and, using whole-body imaging. They found that capillary density increased linearly over 10 days. Similarly, when GFP-expressing MDA-MB-435 cells were orthotopically transplanted to the mouse mammary fat pad, whole-body optical imaging showed that blood vessel density increased linearly over about 20 weeks.

Reversible skin flaps can be used to visualize angiogenesis on GFP-expressing tumors transplanted onto internal organs, in addition to examining the tumor itself (Yang *et al.*, 2002). These angiogenesis mouse models can be used for real-time *in vivo* evaluation of agents inhibiting or promoting tumor angiogenesis (Yang *et al.*, 2001, 2002). Opening a reversible skin-flap in the light path greatly reduces attenuation of the fluorescent signal, thereby increasing the sensitivity of tumor detection by many times. This procedure also greatly increases the depth at which tumor cells can be observed. Single GFP-expressing tumor cells can thus be seen on numerous internal organs. GFP glioma cells seeded on the brain can be visualized through a scalp skin-flap. GFP lung tumor microfoci, which represent a few malignant cells, can be viewed through a skin flap over the chest wall, and contralateral micrometastases can also be examined by use of a corresponding skin flap. Peritoneal wall skin flaps can be used to examine GFP-pancreatic tumors and their angiogenic microvessels. For the liver, a skin flap allowed imaging of physiologically relevant micrometastases that had originated in an orthotopically implanted GFP tumor. Single tumor cells on the liver, which had been introduced through an intraportal injection, were also detectable (Yang *et al.*, 2002).

Ilyin *et al.* (2001) visualized glioma cells in rats by inserting a fiberoptic endoscope through a preimplanted guide cannula. Tumor monitoring was coupled to confocal microscopy so that visualization of the fluorescent signals from the C-6 glioma-GFP cells that had been preimplanted in the brain was

very sensitive. Funovics *et al.* (2003) described the design and construction of a miniaturized multichannel near-infrared endoscopic imaging system developed for high-resolution imaging of mice. This endoscope was used to visualize tumor cells transplanted orthotopically in mice. This device should be useful for *in vivo* imaging using fluorescent proteins (Kelly *et al.*, 2004).

IV. Dual-Color Imaging

GFP- and RFP-labeled HT1080 human fibrosarcoma cells allow the determination of clonality by fluorescence visualization of metastatic colonies after mixed implantation of the red and green fluorescent cells. Resulting pure red or pure green colonies were scored as clonal, whereas mixed yellow colonies were scored as nonclonal. In a spontaneous metastasis model originating from footpad injection in severe combined immunodeficient (SCID) mice, 95% of the resulting lung colonies were either pure green or pure red, indicating monoclonal origin, whereas 5% were of mixed color, indicating polyclonal origin. In an experimental lung metastasis model established by tail vein injection in SCID mice, clonality of lung metastasis was dependent on cell number. With a minimum number of cells was injected, almost all (96%) colonies were pure red or green and therefore monoclonal. When a large number of cells were injected, almost all (87%) colonies were mixed color and therefore heteroclonal. Spontaneous metastases may be clonal because they are rare events, thereby supporting the rare-cell clonal-origin-of-metastasis hypothesis. The clonality of the experimental metastasis model depended on the number of input cells (Yamamoto *et al.*, 2003a).

Dual-color lung metastases were visualized by external fluorescence imaging in live animals through skin flap windows over the chest wall. Lung metastases were observed on the lung surface of all mice. SCID mice tolerated multiple surgical procedures well for direct-view imaging via skin flap windows. Real-time metastatic growth of the two different colored clones in the same lung was externally imaged with resolution and quantification of green, red, or yellow colonies in live animals. The simultaneous real-time dual-color imaging of metastatic colonies gives rise to the possibility of color-coded imaging of clones of cancer cells carrying various forms of gene of interest (Yamamoto *et al.*, 2003b).

V. Dual-Color Tumor–Host Models

A transgenic GFP nude mouse with ubiquitous GFP expression has been developed. The GFP nude mouse was obtained by crossing nontransgenic nude mice with the transgenic C57/B6 mouse in which the β -actin promoter drives GFP expression in essentially all tissues (Okabe *et al.*, 1997). In

crosses between *nu/nu* GFP male mice and *nu/+* GFP female mice, the embryos fluoresced green. Approximately 50% of the offspring of these mice were GFP nude mice. Newborn mice and adult mice fluoresced very bright green and could be detected with a simple blue light-emitting diode flashlight with a central peak of 470 nm and a bypass emission filter. In the adult mice, the organs all brightly expressed GFP, including the heart, lungs, spleen, pancreas, esophagus, stomach, and duodenum. The following systems were dissected out and shown to have brilliant GFP fluorescence: the entire digestive system from tongue to anus; the male and female reproductive systems; the brain and spinal cord; and the circulatory system, including the heart and major arteries and veins. The skinned skeleton highly expressed GFP. Pancreatic islets showed GFP fluorescence. The spleen cells were also GFP positive. RFP-expressing human cancer cell lines, including PC-3-RFP prostate cancer, HCT-116-RFP colon cancer, MDA-MB-435-RFP breast cancer, and HT1080-RFP fibrosarcoma were transplanted to the transgenic GFP nude mice. All of these human tumors grew extensively in the transgenic GFP nude mouse (Yang *et al.*, 2004).

This model shows with great clarity the details of the tumor–stroma interaction, especially tumor-induced angiogenesis and tumor-infiltrating lymphocytes. The GFP-expressing tumor vasculature, both nascent and mature, of the GFP host mouse could be readily distinguished interacting with the RFP-expressing tumor cells. GFP-expressing dendritic cells were observed contacting RFP-expressing tumor cells with their dendrites. GFP-expressing macrophages were observed engulfing RFP-expressing cancer cells. GFP lymphocytes were seen surrounding cells of the RFP tumor, which eventually regressed (Yang *et al.*, 2003).

Duda *et al.* (2004) noted that at the time of transplantation tumor fragments contain “passenger” cells: endothelial cells and other stromal cells from the original host. They investigated the fate of GFP-labeled endothelial and nonendothelial stromal cells after transplantation in syngeneic mice. Angiogenic stroma associated with tumor or adipose tissue persists when transplanted, remains functional, and governed the initial neovascularization of grafted tissue fragments for more than 4 weeks after implantation. The passenger endothelial cells survive longer than other stromal cells, which are replaced by host-activated fibroblasts after 3 weeks. The transplantability of tumor stroma suggests that the angiogenic potential of a tumor xenograft, which determines its viability, depends on the presence of passenger endothelial cells and other stromal cells within the xenograft.

VI. Intravital Imaging of GFP-Expressing Cells

Intravital videomicroscopy can be used to visualize sequential steps in metastasis by use of CHO-K1 cells that stably express GFP. In mouse liver,

the stages from the initial arrest of cells in the microvasculature up to the growth and angiogenesis of metastases have been recorded (Naumov *et al.*, 1999). Individual nondividing cells, as well as micrometastases and macrometastases, were visualized and quantified; additional cellular details such as pseudopodial projections were also detected. Micrometastases were found to preferentially grow and survive near the liver surface. A small population of single cells persisted over the 11-day observation period and the investigators believe these cells may represent dormant tumor cells (Naumov *et al.*, 1999).

GFP techniques have also shown that CT-26 (mouse colon carcinoma) cells inhibit the development of liver metastasis in BALB/c mice that receive intraportal injections of GFP-expressing tumor cells (Guba *et al.*, 2001). Intravital microscopy of the livers of these mice showed that growth of primary tumors promoted dormancy of single tumor cells for up to 7 days. Immunohistological staining for Ki-67 confirmed that these solitary cells were indeed dormant. By contrast, in the absence of a primary tumor, GFP-expressing tumor cells quickly developed into micrometastases. Thus, primary CT-26 tumor implants seem to inhibit tumor metastasis by promotion of a state of single-cell dormancy.

The *ras* oncogene promotes growth of micrometastases into macroscopic metastases. Two types of cells with constitutively active *ras*, NIH 3T3 and T24 H-*ras*-transformed (PAP2) fibroblasts, both of which were expressing GFP, were injected into mouse liver. Subsequent examination by GFP intravital imaging established that only the micrometastases formed by *ras*-transformed cells went on to produce macroscopic metastases; most NIH 3T3 micrometastases just disappeared. Furthermore, PAP2 metastases had a significantly higher proportion of proliferating cells than apoptotic cells, whereas NIH 3T3 metastases had low proliferation and a high proportion of apoptotic cells (Varghese *et al.*, 2002).

VII. Imaging GFP Tumor Cells in Blood Vessels

Following injection of tumor cells stably expressing GFP into the tail vein of mice, it was possible to visualize single tumor cells in blood vessels (Chishima *et al.*, 1997b). With intravital microscopy, Naumov *et al.* (1999) visualized GFP tumor cells colonizing various organs after extravasation. Huang (Huang *et al.*, 1999), Li (Li *et al.*, 2000), and their respective co-workers visualized GFP tumor cell–vessel interaction by use of skin window chambers in rodents and observed angiogenic effects very early in tumor colony formation. In an orthotopic mammary-pad injection model, Wyckoff *et al.* (2000) also visualized tumor–vessel interaction using the fluorescence of the tumor cells. Al-Mehdi *et al.* (2000) saw what they claimed to be

intravascular tumor colony formation by tracking GFP expression in a lung perfusion study. In addition, Moore *et al.* (1998) have also visualized vessels in a GFP-expressing rodent cell line.

Rat tongue carcinoma cell lines expressing GFP have been used to investigate the formation of micrometastasis. The cells were injected into the portal vein and then tracked by use of intravital videomicroscopy (Ito *et al.*, 2001). The two cell types—LM-GFP metastatic and E2-GFP non-metastatic tongue carcinoma cells—immediately got stuck in the sinusoidal vessels near terminal portal venules. The E2-GFP cells disappeared from the liver sinusoid within 3 days, whereas a substantial number of LM-GFP cells remained in the liver, possibly because these cells formed stable attachments to the sinusoidal wall. Upon examination of the process with a confocal laser scanning microscope, only LM-GFP cells were shown to grow in the liver.

Mook *et al.* (2003) noted that initial arrest of colon cancer cells in sinusoids of the liver was due to size restriction after injection of the CC531S-GFP rat tumor cell line. Adhesion of cancer cells to endothelial cells was never found. Instead, endothelial cells retracted rapidly and interactions were observed only between cancer cells and hepatocytes. Tumors developed exclusively intravascularly during the first 4 days. In conclusion, initial steps in the classic metastatic cascade such as adhesion to endothelium and extravasation are not essential for colon cancer metastasis in liver.

Wong *et al.* (2001) showed that death of transformed, metastatic, rat embryo cells, which were expressing GFP, occurred via apoptosis in the lungs 24–48 hours after injection into the circulation. The researchers established that BCL-2 overexpression was causing inhibition of apoptosis in culture, and this mechanism also conferred resistance *in vivo* for 24–48 hours after injection. This inhibition of apoptosis led to a greater number of macroscopic metastases.

Large detectable metastases did not form after athymic mice were given an intravenous injection of chromosome 6–transduced tumor cells expressing GFP (Goldberg *et al.*, 1999). However, fluorescence microscopy revealed micrometastases (single cells or clusters of fewer than 10 cells) in the lungs, suggesting that these cells managed to lodge themselves in the lungs but failed to proliferate. Cells isolated from mouse lungs up to 60 days after the injection were able to grow in culture and formed tumors when injected into skin; therefore, the cells were still viable, but dormant. This result implies that the gene(s) on chromosome 6 interfere specifically with growth-regulatory response in the lung, but not in the skin.

An isogenic pair of metastatic (M4A4) and nonmetastatic (NM2C5), GFP-labeled human breast cancer cell lines derived from the same patient and inoculated into the mammary glands of nude mice was used to visualize the dissemination patterns and fate of cells that escaped spontaneously from the resulting tumors. After tumors appeared, fluorescing single tumor cells

were regularly seen in the lungs, even in animals inoculated with NM2C5, which fails to form secondary tumors in other organs. The sensitivity of the technique confirmed the continuing presence of scattered NM2C5 cells after primary tumor resection, although they formed no metastases by 6 months. These self-disseminated human tumor cells were retrievable from the tissues and were still viable and malignant, manifested by indefinite proliferation *in vitro* and green fluorescence and local tumorigenicity *in vivo*. Therefore, these scattered tumor cells were still alive but rendered indefinitely quiescent by the microenvironmental conditions in the lung tissue. Although many of the cells disseminating from M4A4 tumors grew into fluorescing metastases in the lungs, others remained solitary and quiescent. Therefore, even in a clonally derived cell population with metastatic properties, many cells do not, or cannot, mobilize the organ-specific growth properties needed to generate metastases (Goodison *et al.*, 2003).

Chang *et al.* (2000) used GFP-labeled tumor cells and CD31 and CD105 to identify endothelial cells; they showed that colon carcinoma xenografts had mosaic vessels with focal regions where no CD31/CD105 immunoreactivity was detected and tumor cells appeared to contact the vessel lumen.

Farina *et al.* (1998) developed a model that directly examines the motility of metastatic primary tumor cells *in situ*. A metastatic rat breast cancer cell line was established that constitutively expresses GFP. Animations of metastatic tumor cells moving in the mammary fat pad of live rats were generated by intravital imaging of the primary tumor *in situ* on a laser scanning confocal microscope.

Wyckoff *et al.* (2000) used metastatic (MTLn3) and nonmetastatic (MTC) cell lines derived from the rat mammary adenocarcinoma 13762 NF, expressing GFP to measure tumor cell density in the blood, individual tumor cells in the lungs, and lung metastases. Metastatic cells showed greater orientation toward blood vessels, whereas nonmetastatic cells fragment when interacting with vessels. These results demonstrate that a major difference in intravasation between metastatic and nonmetastatic cells is detected in the primary tumor.

We have recently shown that the neural stem cell marker nestin is expressed in hair follicle stem cells and the blood vessel network interconnecting hair follicles in the skin of transgenic mice with nestin regulatory-element-driven GFP (ND-GFP) (Amoh *et al.*, 2004; Li *et al.*, 2003). The hair follicles were shown to give rise to the nestin-expressing blood vessels in the skin. We also visualized tumor angiogenesis by dual-color fluorescence imaging in ND-GFP transgenic mice after transplantation of the murine melanoma cell line B16F10 expressing RFP. ND-GFP was highly expressed in proliferating endothelial cells and nascent blood vessels in the growing tumor. Results of immunohistochemical staining showed that the blood

vessel-specific antigen CD31 was expressed in ND-GFP-expressing nascent blood vessels. ND-GFP expression was diminished in the vessels with increased blood flow. Progressive angiogenesis during tumor growth was readily visualized during tumor growth by GFP expression. RFP tumor cells were visualized inside ND-GFP blood vessels. Doxorubicin inhibited the nascent tumor angiogenesis as well as tumor growth in the ND-GFP mice transplanted with B16F10-GFP (Amoh *et al.*, 2005).

Yamamoto *et al.* (2004) have genetically engineered dual-color fluorescent cells with one color in the nucleus and the other in the cytoplasm that enables real-time nuclear-cytoplasmic dynamics to be visualized in living cells *in vivo* as well as *in vitro*. Nuclear-GFP expression enabled visualization of nuclear dynamics, whereas simultaneous cytoplasmic RFP expression enabled visualization of nuclear-cytoplasmic ratios as well as simultaneous cell and nuclear shape changes. Thus, total cellular dynamics can be visualized in the living dual-color cells in real time. The cell cycle position of individual living cells was readily visualized by the nuclear-cytoplasmic ratio and nuclear morphology. Real-time induction of apoptosis was observed by nuclear size changes and progressive nuclear fragmentation. Mitotic cells were visualized by whole-body imaging after injection in the mouse ear. Common carotid artery injection of dual-color cells and a reversible skin flap enabled the external visualization of the dual-color cells in microvessels in the mouse brain where extreme elongation of the cell body as well as the nucleus occurred. Dual-color cells in various positions of the cell cycle were visualized in excised mouse lungs after tail vein injection of the dual-color cells. In the lung, the dual-color cells were observed frequently juxtaposing their nuclei, suggesting a potential novel form of cell-cell communication.

After the dual-color HT1080 cells were injected in the hearts of nude mice, a skin-flap on the abdomen was made and spread on a flat stand. Highly elongated cancer cells were observed in capillaries in the skin-flap in living mice with a color charge-coupled device (CCD) camera. The migration velocities of the cancer cells in the capillaries were measured by capturing images of the dual-color fluorescent cells over time. The cells in the capillaries elongated to fit the width of these vessels. The average length of the major axis of the cancer cells in the capillaries increased to 3.97 times their normal length. The nuclei increased their length 1.64 times in the capillaries. Cancer cells that were arrested in capillaries more than 8 μm in diameter could migrate up to 48.3 $\mu\text{m}/\text{hr}$. The data suggest that the minimum diameter of capillaries where cancer cells are able to migrate is approximately 8 μm . Extravasation was found to be infrequent in the HT1080 cells, which were visualized by dual-color imaging to be frequently undergoing apoptosis. Mouse mammary tumor cells, in contrast, frequently extravasated beginning approximately 18 hours after cell injection. The cytoplasm of the

MMT cells exited the vessels first and subsequently the whole cancer cell extravasated. The use of the dual-color cancer cells differentially labeled in the cytoplasm and nucleus and associated fluorescence imaging provide a powerful tool to understand the mechanism of cancer cell migration and deformation in small vessels and extravasation (Yamauchi *et al.*, 2005; Yamauchi, K. and Hoffman, R. M., unpublished data).

VIII. Clinically Applicable Models of GFP Tumor Imaging

Several studies have focused on delivering the GFP gene selectively to tumors in order to provide a marker for the development of new metastases. Hasegawa *et al.* (2000) administered the GFP gene to nude mice with human stomach tumors growing intraperitoneally in order to visualize future regional and distant metastases. GFP retroviral supernatants were injected intraperitoneally from day 4 to day 10 following implantation of the cancer cells. A laparotomy was done every other week so that tumor growth and metastasis formation could be visualized by GFP expression. No normal tissues were transduced by the GFP retrovirus. Two weeks after retroviral GFP delivery, GFP-expressing tumor cells were observed in the gonadal fat, greater omentum, and intestine, indicating that the tumors were efficiently transduced by the GFP gene and could be detected by its expression. Second and third laparotomies were done at weeks 4 and 6, respectively. GFP-expressing tumor cells were found spreading to lymph nodes in the mesentery. The fourth laparotomy, at 8 weeks, showed widespread GFP-expressing tumor growth including metastasis to the liver. Thus, reporter gene transduction of the primary tumor enabled detection of its subsequent metastasis. This reporter gene therapy model could be applied to primary tumors before resection or other treatment and thus provide an early detection system for metastasis and recurrence (Hasegawa *et al.*, 2000).

Human MKN45-GFP stomach cancer cells were injected into the peritoneal cavity of BALB/c nude mice to determine whether the carcinoembryonic antigen promoter could direct the GFP gene to the tumor (Kaneko *et al.*, 2001). A carcinoembryonic antigen (CEA) enhanced fluorescent protein (EGFP) plasmid was thus introduced in the peritoneal cavity using liposomes. GFP-fluorescent tumor nodules were subsequently detected by fluorescence stereomicroscopy.

In another approach, a GFP gene was conjugated to transferrin to target disseminated tumors *in vivo* (Sato *et al.*, 2000). When GFP gene conjugates were systemically administered through the tail vein to nude mice that had been subcutaneously inoculated with tumor, GFP expression was detected only in the tumor.

Varda-Bloom *et al.* (2001) developed a tissue-specific gene therapy to the angiogenic blood vessels of tumor metastasis using an adeno-based vector containing the murine preproendothelin-1 (PPE-1) promoter driving GFP. High specific activity of PPE-1 was achieved by systemic administration of the adenoviral vector to mice bearing Lewis lung carcinoma tumors. This effect was detected by GFP expression in the new vasculature of primary tumors and lung metastasis. The highest area of expression was in the angiogenic endothelial cells of the metastasis.

GFP on a herpes simplex virus type 1–Epstein-Barr virus (HSV-1/EBV) vector has been administered to tumor-bearing animals. However, persistent GFP expression was not achieved in this study (Qi *et al.*, 2000).

Umeoka *et al.* (2004) described a new approach to visualizing tumors whose fluorescence can be detected using tumor-specific replication-competent adenovirus in combination with Ad-GFP, a replication-deficient adenovirus expressing GFP. An adenovirus 5 vector (OBP-301) was constructed in which the human telomerase reverse transcriptase promoter element drives expression of E1A and E1B genes linked with an internal ribosome entry site. When human lung and colon cancer cell lines were infected with Ad-GFP at a low multiplicity of infection, GFP expression could not be detected. In the presence of OBP-301, however, Ad-GFP replicated in these tumor cells and showed strong green signals. In contrast, co-infection with OBP-301 and Ad-GFP did not show any signals in normal cells such as fibroblasts and vascular endothelial cells. Subcutaneous tumors could be visualized after intratumoral injection of OBP-301 and Ad-GFP in nude mice. Within 3 days of treatment, the fluorescence of the expressed GFP became visible. Intrathoracic administration of Ad-GFP and OBP-301 could visualize disseminated A549 tumor nodules in mice after intrathoracic implantation.

IX. Fluorescent Reporter Gene for Human T Cells

Normal, human, peripheral blood T lymphocytes were transduced with a retroviral herpes simplex virus–thymidine kinase (HSV-TK-GFP; vGFPTKfus) and nucleus-restricted green fluorescence was observed. Sorting allowed for selection of GFP-expressing T lymphocytes. The ability to target GFP-expressing T lymphocytes to tumors could have many clinical uses (Paquin *et al.*, 2001).

Singbartl *et al.* (2001) described the development of a CD2-enhanced GFP-transgenic mouse to characterize lymphocyte trafficking. A CD2-GFP plasmid including the CD2 promoter, the GFP transgene, and the CD2 locus control region was injected into B6CBA/F1 pronuclei to con-

struct the transgenic mice. GFP CD8⁺ T cells were imaged in cremaster muscle venules treated with both tumor necrosis factor- α and interferon- γ .

Panoskaltis-Mortari *et al.* (2004) developed a mouse system in which to track the migration and homing of cells in a setting of bone marrow transplantation-induced graft-versus-host disease (GVHD). After systemic infusion using GFP cells, a fluorescence stereomicroscope outfitted with a color CCD camera was used for imaging. Whole-body images of anesthetized mice taken at various time points after cell infusion revealed the early migration of allogeneic cells to peripheral lymphoid organs, with later infiltration of GVHD target organs. Localization of GFP cells could be seen through the skin of shaved mice, and internal organs were easily discernible. After allogeneic or syngeneic GFP cell infusion, representative mice were dissected to better visualize deeper internal organs and tissues. Infusion of different cell populations revealed distinct homing patterns. This method thus provides a simple way to identify the critical time points for expansion of the transplanted cells in various organs.

X. Bone Marrow Protection by Transfer of Drug-Resistance Genes Coupled to GFP

A retroviral vector expressing human O⁶-methylguanine-DNA methyltransferase (MGMT) and GFP was developed for stem cell protection in a murine transplant model. Mice transplanted with transduced cells showed significant resistance to the myelosuppressive effects of temozolomide, a DNA-methylating drug, and O⁶-benzylguanine, a drug that inhibits MGMT. Following drug treatment, increases in GFP-positive peripheral blood cells were seen. Secondary transplant experiments proved that selection had occurred at the stem cell level. Such an approach could be used clinically in the future to protect bone marrow against chemotherapy (Sawai *et al.*, 2001).

XI. Molecular Imaging

p53 tumor-suppressor functions were visualized *in vivo* by GFP imaging. By use of the antiapoptotic gene *BCL-2* or a dominant-negative caspase 9 (*C9DN*), GFP whole-body imaging established that disruption of the apoptosis pathway downstream of p53 leads to *E μ -myc-GFP* lymphoma expansion that phenocopies p53 loss in *E μ -myc* transgenic mice. This finding shows that GFP whole-body imaging can be used to identify

individual genes that affect tumor growth. Such information could be used to identify genes predicting aggressive tumor growth (Schmitt *et al.*, 2002a).

XII. Chemotherapy Effects of a Senescence Program Controlled by p53 and p16^{INK4a}

The GFP primary lymphomas derived from *Eμ-myc* transgenic mice respond to chemotherapy by undergoing apoptosis and engaging a premature senescence program controlled by p53 and p16^{INK4a}. Therefore, tumors respond poorly to cyclophosphamide therapy if their p53 or *INK4a/ARF* genes are disrupted; this can be seen with GFP whole-body imaging. It has also been shown that mice bearing tumors capable of drug-induced senescence have a much better prognosis after chemotherapy than those harboring tumors with senescence defects. These findings indicated that premature senescence can contribute to treatment outcome *in vivo* and provide new insights into the molecular genetics of drug resistance, which can be applied clinically (Schmitt *et al.*, 2002b).

XIII. Conclusions and Future Directions

Tumor cells stably expressing GFP *in vivo* are a powerful new tool for cancer research. Stability of expression has been studied by Naumov *et al.* (1999), who noted that all the CHO-K1-GFP cells used in their study were stably fluorescent (measured by flow cytometry) even after 24 days of growing in medium where they were deprived of selective pressure. This finding implies that GFP can be stably expressed in cells *in vivo*. This feature has proved true for all cells studied so far and is exemplified by the generation of extensive GFP-expressing metastases.

The use of GFP-expressing tumor cells in transplanted mice, fresh tissue, or live animals (Chishima *et al.*, 1997b; Naumov *et al.*, 1999) has provided new insights into the real-time growth and metastatic behavior of cancer. Several independent studies, which include an extensive comparison between metastases of GFP-transduced rat mammary carcinoma cell and the parental cell line (Chishima *et al.*, 1997b,d; Farina *et al.*, 1998) have shown that GFP transduction and expression does not affect metastatic behavior. GFP can be transfected into any cell type of interest and used as a cytoplasmic marker to show the general outlines of cells *in vivo* as well as fine morphological details such as long slender pseudopodial projections (Naumov *et al.*, 1999).

The development of tumor cells that stably express GFP at high levels has enabled investigation of tumor and metastatic growth in a completely noninvasive manner by use of whole-body imaging (Yang *et al.*, 2000). For the first time, tumor growth and metastatic studies, including drug evaluations, can be done and quantified in real time in nonperturbed individual animals. The potential of this technology is very high.

A further advantage of GFP-expressing cells is the increased contrast between brightly fluorescent tumor tissue and blood vessels within it. The ability to visualize and quantify blood-vessel development in metastases *in vivo* will greatly facilitate studies of angiogenesis and the testing of effects of antiangiogenic agents on metastatic development (Naumov *et al.*, 1999; Yang *et al.*, 2001).

The GFP approach has several important advantages over other optical approaches to imaging. In comparison with the luciferase reporter, GFP has a much stronger signal and therefore can be used to image unrestrained animals. The fluorescence intensity of GFP is very strong since the quantum yield is approximately 0.9 (Cormack *et al.*, 1996; Cramer *et al.*, 1996; Delagrave *et al.*, 1995; Heim *et al.*, 1995; Morin and Hastings, 1971). The protein sequence of GFP has also been "humanized," which enables it to be highly expressed in mammalian cells (Zolotukhin *et al.*, 1996). In addition, GFP fluorescence is fairly unaffected by the external environment since the chromophore is protected by the three-dimensional structure of the protein (Cody *et al.*, 1993). *In vivo*, GFP fluorescence is mainly limited by light scattering which, as noted previously, can be overcome by skin flaps (Yang *et al.*, 2002) and endoscopes (Ilyin *et al.*, 2001) so that single cells can be imaged externally. Longer-wavelength fluorescence proteins, such as RFP, can also be used to reduce scatter.

An improved method of whole-body GFP imaging made use of a laser excitation source and band-pass filters matched specifically to GFP and constitutive tissue fluorescence emission bands. Processing of the primary GFP fluorescence images acquired by a CCD camera subtracted background tissue autofluorescence. This approach achieved 100% sensitivity and specificity for *in vivo* detection of a 10%-transfected BxPC3 pancreatic tumor after subcutaneous grafting or orthotopic implantation in the pancreas of nude mice (Wack *et al.*, 2003).

The luciferase reporter technique requires that animals be anesthetized and restrained so that sufficient photons to construct an image can be collected. Furthermore, this process must be carried out in a virtually light-free environment and animals must be injected with the luciferin substrate, which must reach every tumor cell in order to be useful. This limitation precludes studies that would be perturbed by anesthesia, restraint, or substrate injection and also makes high-throughput screening

unfeasible. Expression of firefly luciferase (Luc) can be used to visualize tumor cell growth and regression in response to various therapies in mice. However, detection of Luc-labeled cells *in vivo* was limited to 1000 human tumor cells (Contag *et al.*, 2000; Sweeney *et al.*, 1999). The clearance of the luciferin results in an unstable luciferase signal (Burgos *et al.*, 2003). The high-intensity signal produced by GFP, however, allows unrestrained animals to be imaged without any perturbation or substrate—irradiation with nondamaging blue light is the only step needed. Images can be captured with fairly simple apparatus and there is no need for darkness.

A fusion vector containing the luciferase gene, the monomeric RFP gene, and the herpes simplex thymidine kinase gene was tested *in vivo*. A highly sensitive cooled CCD camera compatible with both luciferase and fluorescence imaging compared these two signals from the fused reporter gene using a lentivirus vector in 293T cells implanted in nude mice. The signal from RFP was approximately 1000 times stronger than luciferase (Ray *et al.*, 2004).

Near-infrared probes activated by the action of proteases (Bremer *et al.*, 2001; Weissleder *et al.*, 1999) can also be used for optical imaging of tumors. This approach requires substrate injection and the tumor must contain a specific protease that cleaves the substrate. Tumors on normal tissues (e.g., the liver) that contain these proteases cannot be visualized because background signals are too high; there is not sufficient distinction between tumor and normal tissue to obtain useful external images (Hirsch *et al.*, 2001).

For clinical application of GFP developments, future studies may make use of the approach of Hasegawa *et al.* (2000), who used retroviral GFP vectors that were selectively targeted to tumors for the purpose of identifying future metastasis. GFP labeling of tumor-infiltrating lymphocytes (Paquin *et al.*, 2001) and bone marrow transduced with GFP-linked genes that confer chemoresistance (Sawai *et al.*, 2001) also have intriguing clinical potential. Umeoka *et al.* (2004) have shown that intratumoral or intrathoracic administration of Ad-GFP in combination with another vector containing a telomerase promoter driving the E1A and E1B genes could possibly be used clinically in the future to label tumors with GFP.

The applications of *in vivo* cellular imaging with fluorescent proteins should markedly expand with the development of proteins with new colors. Tsien *et al.* (2004) have taken the *Discoma* RFP and converted it through multiple amino acid substitutions into a monomer. With further genetic modification this group has created from the *Discoma* RFP monomer a series of modified proteins with multiple new colors from yellow-orange to red-orange. These new colored proteins include mBanana, mOrange, dTomato, tdTomato, mTangerine, mStrawberry, and mCherry with increasingly longer emission maxima. It is expected that many additional colored proteins will be isolated from various organisms and modified to

produce even more colors. The availability of large number of different colored proteins will enable simultaneous imaging of multiple cellular events *in vivo*.

Acknowledgments

These studies were supported in part by National Cancer Institute grants CA99258, CA101600, and CA103563.

References

- Al-Mehdi, A. B., Tozawa, K., Fisher, A. B., Shientag, L., Lee, A., and Muschel, R. J. (2000). Intravascular origin of metastasis from the proliferation of endothelium-attached tumor cells: A new model for metastasis. *Nat. Med.* **6**, 100–102.
- Amoh, Y., Li, L., Yang, M., Moossa, A. R., Katsuoka, K., Penman, S., and Hoffman, R. M. (2004). Nascent blood vessels in the skin arise from nestin-expressing hair follicle cells. *Proc. Natl. Acad. Sci. USA* **101**, 13291–13295.
- Amoh, Y., Li, L., Yang, M., Jiang, P., Moossa, A. R., Katsuoka, K., and Hoffman, R. M. (2005). Hair-follicle-derived blood vessels vascularize tumors in skin and are inhibited by doxorubicin. *Cancer Res.* **65**, 2337–2343.
- Bouvet, M., Wang, J. W., Nardin, S. R., Nassirpour, R., Yang, M., Baranov, E., Jiang, P., Moossa, A. R., and Hoffman, R. M. (2002). Real-time optical imaging of primary tumor growth and multiple metastatic events in a pancreatic cancer orthotopic model. *Cancer Res.* **62**, 1534–1540.
- Bouvet, M., Yang, M., Nardin, S., Wang, X., Jiang, P., Baranov, E., Moossa, A. R., and Hoffman, R. M. (2000). Chronologically-specific metastatic targeting of human pancreatic tumors in orthotopic models. *Clin. Exp. Metastasis* **18**, 213–218.
- Bremer, C., Tung, C. H., and Weissleder, R. (2001). *In vivo* molecular target assessment of matrix metalloproteinase inhibition. *Nat. Med.* **7**, 743–748.
- Brown, E. B., Campbell, R. B., Tsuzuki, Y., Xu, L., Carmeliet, P., Fukumura, D., and Jain, R. K. (2001). *In vivo* measurement of gene expression, angiogenesis and physiological function in tumors using multiphoton laser scanning microscopy. *Nat. Med.* **7**, 864–868.
- Burgos, J. S., Rosol, M., Moats, R. A., Khankaldyyan, V., Kohn, D. B., Nelson, M. D., Jr., and Laug, W. E. (2003). Time course of bioluminescent signal in orthotopic and heterotopic brain tumors in nude mice. *Biotechniques* **34**, 1184–1188.
- Chang, Y. S., di Tomaso, E., McDonald, D. M., Jones, R., Jain, R. K., and Munn, L. L. (2000). Mosaic blood vessels in tumors: Frequency of cancer cells in contact with flowing blood. *Proc. Natl. Acad. Sci. USA* **97**, 14608–14613.
- Chaudhuri, T. R., Mountz, J. M., Rogers, B. E., Partridge, E. E., and Zinn, K. R. (2001). Light-based imaging of green fluorescent protein-positive ovarian cancer xenografts during therapy. *Gynecol. Oncol.* **82**, 581–589.
- Chaudhuri, T. R., Cao, Z., Krasnykh, V. N., Stargel, A. V., Belousova, N., Partridge, E. E., and Zinn, K. R. (2003). Blood-based screening and light based imaging for the early detection and monitoring of ovarian cancer xenografts. *Technol. Cancer Res. Treat.* **2**, 171–180.

- Chishima, T., Miyagi, Y., Wang, X., Yamaoka, H., Shimada, H., Moossa, A. R., and Hoffman, R. M. (1997b). Cancer invasion and micrometastasis visualized in live tissue by green fluorescent protein expression. *Cancer Res.* **57**, 2042–2047.
- Chishima, T., Miyagi, Y., Wang, X., Baranov, E., Tan, Y., Shimada, H., Moossa, A. R., and Hoffman, R. M. (1997c). Metastatic patterns of lung cancer visualized live and in process by green fluorescent protein expression. *Clin. Exp. Metastasis* **15**, 547–552.
- Chishima, T., Miyagi, Y., Wang, X., Tan, Y., Shimada, H., Moossa, A., and Hoffman, R. M. (1997d). Visualization of the metastatic process by green fluorescent protein expression. *Anticancer Res.* **17**, 2377–2384.
- Chishima, T., Yang, M., Miyagi, Y., Li, L., Tan, Y., Baranov, E., Shimada, H., Moossa, A. R., Penman, S., and Hoffman, R. M. (1997). Governing step of metastasis visualized *in vitro*. *Proc. Natl. Acad. Sci. USA* **94**, 11573–11576.
- Choy, G., O' Connor, S., Diehn, F. E., Costouros, N., Alexander, H. R., Choyke, P., and Libutti, S. K. (2003). Comparison of noninvasive fluorescent and bioluminescent small animal optical imaging. *Biotechniques* **35**, 1022–1026, 1028–1030.
- Cody, C. W., Prasher, D. C., Westler, V. M., Prendergast, F. G., and Ward, W. W. (1993). Chemical structure of the hexapeptide chromophore of the *Aequorea* green fluorescent protein. *Biochemistry* **32**, 1212–1218.
- Contag, C. H., Jenkins, D., Contag, P. R., and Negrin, R. S. (2000). Use of reporter genes for optical measurements of neoplastic disease *in vivo*. *Neoplasia* **2**, 41–52.
- Cormack, B., Valdivia, R., and Falkow, S. (1996). FACS-optimized mutants of the green fluorescent protein (GFP). *Gene* **173**, 33–38.
- Cramer, A., Whitehorn, E. A., Tate, E., and Stemmer, W. P. C. (1996). Improved green fluorescent protein by molecular evolution using DNA shuffling. *Nat. Biotechnol.* **14**, 315–319.
- Delgrave, S., Hawtin, R. E., Silva, C. M., Yang, M. M., and Youvan, D. C. (1995). Red-shifted excitation mutants of the green fluorescent protein. *Biotechnology* **13**, 151–154.
- Duda, D. G., Fukumura, D., Munn, L. L., Booth, M. F., Brown, E. B., Huang, P., Seed, B., and Jain, R. K. (2004). Differential transplantability of tumor-associated stromal cells. *Cancer Res.* **64**, 5920–5924.
- Farina, K. L., Wyckoff, J. B., Rivera, J., Lee, H., Segall, J. E., Condeelis, J. S., and Jones, J. G. (1998). Cell motility of tumor cells visualized in living intact primary tumors using green fluorescent protein. *Cancer Res.* **58**, 2528–2532.
- Fukumura, D., Yuan, F., Monsky, W. L., Chen, Y., and Jain, R. K. (1997). Effect of host microenvironment on the microcirculation of human colon adenocarcinoma. *Am. J. Pathol.* **151**, 679–988.
- Fukumura, D., Xavier, R., Sugiura, T., Chen, Y., Park, E. C., Lu, N., Selig, M., Nielsen, G., Taksir, T., Jain, R. K., and Seed, B. (1998). Tumor induction of VEGF promoter activity in stromal cells. *Cell* **94**, 715–725.
- Funovics, M. A., Alencar, H., Su, H. S., Khazaie, K., Weissleder, R., and Mahmood, U. (2003). Miniaturized multichannel near infrared endoscope for mouse imaging. *Mol. Imaging* **2**, 350–357.
- Goldberg, S. F., Harms, J. F., Quon, K., and Welch, D. R. (1999). Metastasis-suppressed C8161 melanoma cells arrest in lung but fail to proliferate. *Clin. Exp. Metastasis* **17**, 601–607.
- Goodison, S., Kawai, K., Hihara, J., Jiang, P., Yang, M., Urquidi, V., Hoffman, R. M., and Tarin, D. (2003). Prolonged dormancy and site-specific growth potential of cancer cells spontaneously disseminated from nonmetastatic breast tumors as revealed by labeling with green fluorescent protein. *Clin. Cancer Res.* **9**, 3808–3814.
- Guba, M., Cernaianu, G., Koehi, G., Geissler, E. K., Jauch, K. W., Anthuber, M., Falk, W., and Steinbauer, M. (2001). A primary tumor promotes dormancy of solitary tumor cells before inhibiting angiogenesis. *Cancer Res.* **61**, 5575–5579.

- Harms, J. F., and Welch, D. R. (2003). MDA-MB-435 human breast carcinoma metastasis to bone. *Clin. Exp. Metastasis* **20**, 327–334.
- Hasegawa, S., Yang, M., Chishima, T., Miyagi, Y., Shimada, H., Moossa, A. R., and Hoffman, R. M. (2000). *In vivo* tumor delivery of the green fluorescent protein gene to report future occurrence of metastasis. *Cancer Gene Ther.* **7**, 1336–1340.
- Hastings, R. H., Burton, D. W., Quintana, R. A., Biederman, E., Gujral, A., and Deftos, L. J. (2001). Parathyroid hormone-related protein regulates the growth of orthotopic human lung tumors in athymic mice. *Cancer* **92**, 1402–1410.
- Heim, R., Cubitt, A. B., and Tsien, R. Y. (1995). Improved green fluorescence. *Nature* **373**, 663–664.
- Hirsch, F. R., Prindiville, S. A., Miller, Y. E., Franklin, W. A., Dempsey, E. C., Murphy, J. R., Bunn, P. A., Jr., and Kennedy, T. C. (2001). Fluorescence versus white-light bronchoscopy for detection of preneoplastic lesions: A randomized study. *J. Natl. Cancer Inst.* **93**, 1385–1391.
- Huang, M. S., Wang, T. J., Liang, C. L., Huang, H. M., Yang, I. C., Yi-Jan, H., and Hsiao, M. (2002). Establishment of fluorescent lung carcinoma metastasis model and its real-time microscopic detection in SCID mice. *Clin. Exp. Metastasis* **19**, 359–368.
- Huang, Q., Shan, S., Braun, R. D., Lanzen, J., Anyrhambatla, G., Kong, G., Borelli, M., Corry, P., Dewhirst, M. W., and Li, C. Y. (1999). Noninvasive visualization of tumors in rodent dorsal skin window chambers. *Nat. Biotechnol.* **17**, 1033–1035.
- Ilyin, S. E., Flynn, M. C., and Plata-Salaman, C. R. (2001). Fiber-optic monitoring coupled with confocal microscopy for imaging gene expression *in vitro* and *in vivo*. *J. NeuroSci. Methods* **108**, 91–96.
- Ito, S., Nakanishi, H., Ikehara, Y., Kato, T., Kasai, Y., Ito, K., Akiyama, S., Nakao, A., and Tatematsu, M. (2001). Real-time observation of micrometastasis formation in the living mouse liver using a green fluorescent protein gene-tagged rat tongue carcinoma cell line. *Int. J. Cancer* **93**, 212–217.
- Kaneko, K., Yano, M., Yamano, T., Tsujinaka, T., Miki, H., Akiyama, Y., Taniguchi, M., Fujiwara, Y., Doki, Y., Inoue, M., Shiozaki, H., Kaneda, Y., and Monden, M. (2001). Detection of peritoneal micrometastases of gastric carcinoma with green fluorescent protein and carcinoembryonic antigen promoter. *Cancer Res.* **61**, 5570–5574.
- Katz, M. H., Bouvet, M., Takimoto, S., Spivack, D., Moossa, A. R., and Hoffman, R. M. (2003b). Selective antimetastatic activity of cytosine analog CS-682 in a red fluorescent protein orthotopic model of pancreatic cancer. *Cancer Res.* **63**, 5521–5525.
- Katz, M. H., Bouvet, M., Takimoto, S., Spivack, D., Moossa, A. R., and Hoffman, R. M. (2004). Survival efficacy of adjuvant cytosine-analogue CS-682 in a fluorescent orthotopic model of human pancreatic cancer. *Cancer Res.* **64**, 1828–1833.
- Katz, M. H., Takimoto, S., Spivack, D., Moossa, A. R., Hoffman, R. M., and Bouvet, M. (2003). A novel red fluorescent protein orthotopic pancreatic cancer model for the preclinical evaluation of chemotherapeutics. *J. Surg. Res.* **113**, 151–160.
- Kelly, K., Alencar, H., Funovics, M., Mahmood, U., and Weissleder, R. (2004). Detection of invasive colon cancer using a novel, targeted, library-derived fluorescent peptide. *Cancer Res.* **64**, 6247–6251.
- Li, C. Y., Shan, S., Huang, Q., Braun, R. D., Lanzen, J., Hu, K., Lin, P., and Dewhirst, M. W. (2000). Initial stages of tumor cell-induced angiogenesis: Evaluation via skin window chambers in rodent models. *J. Natl. Cancer Inst.* **92**, 143–147.
- Li, L., Mignone, J., Yang, M., Matic, M., Penman, S., Enikolopov, G., and Hoffman, R. M. (2003). Nestin expression in hair follicle sheath progenitor cells. *Proc. Natl. Acad. Sci. USA* **100**, 9958–9961.
- Maeda, H., Segawa, T., Kamoto, T., Yoshida, H., Kakizuka, A., Ogawa, O., and Kakehi, Y. (2000). Rapid detection of candidate metastatic foci in the orthotopic inoculation model of

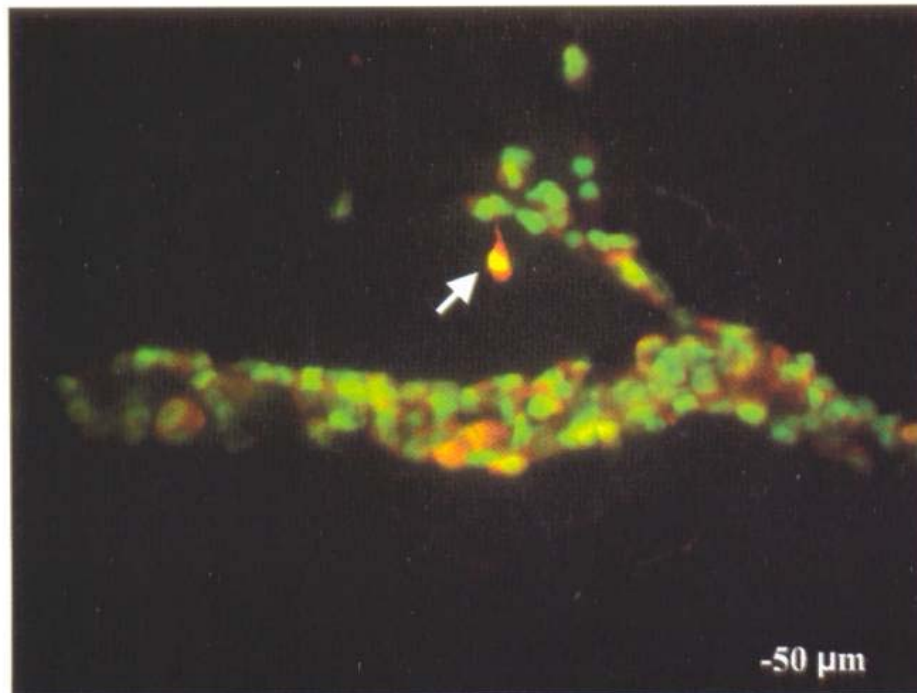
- androgen-sensitive prostate cancer cells introduced with green fluorescent protein. *Prostate* **45**, 335–340.
- Matz, M. V., Fradkov, A. F., Labas, Y. A., Savitsky, A. P., Zaraisky, A. G., Markelov, M. L., and Lukyanov, S. A. (1999). Fluorescent proteins from nonbioluminescent *Anthozoa* species. *Nat. Biotechnol.* **17**, 969–973.
- Mook, O. R., Van Marle, J., Vreeling-Sindelarova, H., Jonges, R., Frederiks, W. M., and Van Noorden, C. J. (2003). Visualization of early events in tumor formation of eGFP-transfected rat colon cancer cells in liver. *Hepatology* **38**, 295–304.
- Moore, A., Marecos, E., Simonova, M., Weissleder, R., and Bogdanov, A., Jr. (1998). Novel gliosarcoma cell line expressing green fluorescent protein: A model for quantitative assessment of angiogenesis. *Microvasc Res.* **56**, 145–153.
- Morin, J., and Hastings, J. (1971). Energy transfer in a bioluminescent system. *J. Cell Physiol.* **77**, 313–318.
- Naumov, G. N., Wilson, S. M., MacDonald, I. C., Schmidt, E. E., Morris, V. L., Groom, A. C., Hoffman, R. M., and Chambers, A. F. (1999). Cellular expression of green fluorescent protein, coupled with high-resolution *in vivo* videomicroscopy, to monitor steps in tumor metastasis. *J. Cell Sci.* **112**, 1835–1842.
- Okabe, M., Ikawa, M., Kominami, K., Nakanishi, T., and Nishimune, Y. (1997). 'Green mice' as a source of ubiquitous green cells. *FEBS Lett.* **407**, 313–319.
- Panoskaltis-Mortari, A., Price, A., Hermanson, J. R., Taras, E., Lees, C., Serody, J. S., and Blazar, B. R. (2004). *In vivo* imaging of graft-versus-host-disease in mice. *Blood* **103**, 3590–3598.
- Paquin, A., Jaalouk, D. E., and Galipeau, J. (2001). Retrovector encoding a green fluorescent protein-herpes simplex virus thymidine kinase fusion protein serves as a versatile suicide/reporter for cell and gene therapy applications. *Hum. Gene Ther.* **12**, 13–23.
- Peyruchaud, O., Winding, B., Pecheur, I., Serre, C. M., Delmas, P., and Clezardin, P. (2001). Early detection of bone metastases in a murine model using fluorescent human breast cancer cells: Application to the use of the bisphosphonate zoledronic acid in the treatment of osteolytic lesions. *J. Bone Miner. Res.* **16**, 2027–2034.
- Qi, J., Link, C. J., Jr., and Wang, S. (2000). Direct observation of GFP gene expression transduced with HSV-1/EBV amplicon vector in unfixed tumor tissue. *Biotechniques* **28**, 206–208.
- Rashidi, B., Yang, M., Jiang, P., Baranov, E., An, Z., Wang, X., Moossa, A. R., and Hoffman, R. M. (2000). A highly metastatic Lewis lung carcinoma orthotopic green fluorescent protein model. *Clin. Exp. Metastasis* **18**, 57–60.
- Ray, P., De, A., Min, J-J, Tsien, R. Y., and Gambhir, S. S. (2004). Imaging tri-fusion multimodality reporter gene expression in living subjects. *Cancer Res.* **64**, 1323–1330.
- Sato, Y., Yamauchi, N., Takahashi, M., Sasaki, K., Fukaura, J., Neda, H., Fujii, S., Hirayama, M., Itoh, Y., Koshita, Y., Kogawa, K., Kato, J., Sakamaki, S., and Niitsu, Y. (2000). *In vivo* gene delivery to tumor cells by transferrin-streptavidin-DNA conjugate. *FASEB J.* **14**, 2108–2118.
- Sawai, N., Zhou, S., Vanin, E. F., Houghton, P., Brent, T. P., and Sorrentino, B. P. (2001). Protection and *in vivo* selection of hematopoietic stem cells using temozolomide, O6-benzylguanine, and an alkyltransferase-expressing retroviral vector. *Mol. Ther.* **3**, 78–87.
- Schmitt, C. A., Fridman, J. S., Yang, M., Baranov, E., Hoffman, R. M., and Lowe, S. W. (2002a). Dissecting p53 tumor suppressor functions *in vivo*. *Cancer Cell* **1**, 289–298.
- Schmitt, C. A., Fridman, J. S., Yang, M., Lee, S., Baranov, E., Hoffman, R. M., and Lowe, S. W. (2002b). Senescence program controlled by p53 and p16 INK4a contributes to the outcome of cancer therapy. *Cell* **109**, 335–346.

- Singbartl, K., Thatte, J., Smith, M. L., Wethmar, K., Day, K., and Ley, K. (2001). A CD2-green fluorescence protein-transgenic mouse reveals very late antigen-4-dependent CD8+ lymphocyte rolling in inflamed venules. *J. Immunol.* **166**, 7520–7526.
- Sweeney, T. J., Mailander, V., Tucker, A. A., Olomu, A. B., Zhang, W., Cao, Y., Negrin, R. S., and Contag, C. H. (1999). Visualizing the kinetics of tumor-cell clearance in living animals. *Proc. Natl. Acad. Sci. USA* **96**, 12044–12049.
- Umeoka, T., Kawashima, T., Kagawa, S., Teraishi, F., Taki, M., Nishizaki, M., Kyo, S., Nagai, K., Urata, Y., Tanaka, N., and Fujiwara, T. (2004). Visualization of intrathoracically disseminated solid tumors in mice with optical imaging by telomerase-specific amplification of a transferred green fluorescent protein gene. *Cancer Res.* **64**, 6259–6265.
- Varda-Bloom, N., Shaish, A., Gonen, A., Levanon, K., Greenbereger, S., Ferber, S., Levkovitz, H., Castel, D., Goldberg, I., Afek, A., Kopolovitch, Y., and Harats, D. (2001). Tissue-specific gene therapy directed to tumor angiogenesis. *Gene Ther.* **8**, 819–827.
- Varghese, H. J., Davidson, M. T., Mac Donald, I. C., Wilson, S. M., Nadkarni, K. V., Groom, A. C., and Chambers, A. F. (2002). Activated ras regulates the proliferation/apoptosis balance and early survival of developing micrometastases. *Cancer Res.* **62**, 887–891.
- Wack, S., Hajri, A., Heisel, F., Sowinska, M., Berger, C., Whelan, M., Marescaux, J., and Aprahamian, M. (2003). Feasibility, sensitivity, and reliability of laser-induced fluorescence imaging of green fluorescent protein-expressing tumors *in vivo*. *Mo. Ther.* **7**, 765–773.
- Wang, J., Yang, M., and Hoffman, R. M. (2004). Visualizing portal vein metastatic trafficking to the liver with green fluorescent protein-expressing tumor cells. *Anticancer Res.* **24**, 3699–3702.
- Weissleder, R., Tung, C. H., Mahmood, U., and Bogdanov, A., Jr. (1999). *In vivo* imaging of tumors with protease-activated near-infrared fluorescent probes. *Nat. Biotechnol.* **17**, 375–378.
- Wong, C. W., Lee, A., Shientag, L., Yu, J., Dong, Y., Kao, G., Al-Mehdi, A. B., Bernhard, E. J., and Muschel, R. J. (2001). Apoptosis: An early event in metastatic inefficiency. *Cancer Res.* **61**, 333–338.
- Wyckoff, J. B., Jones, J. G., Condeelis, J. S., and Segall, J. E. (2000). A critical step in metastasis: *In vivo* analysis of intravasation at the primary tumor. *Cancer Res.* **60**, 2504–2511.
- Yamamoto, N., Jiang, P., Yang, M., Xu, M., Yamauchi, K., Tsuchiya, H., Tomita, K., Wahl, G. M., Moossa, A. R., and Hoffman, R. M. (2004). Cellular dynamics visualized in live cells *in vitro* and *in vivo* by differential dual-color nuclear-cytoplasmic fluorescent-protein expression. *Cancer Res.* **64**, 4251–4256.
- Yamamoto, N., Yang, M., Jiang, P., Xu, M., Tsuchiya, H., Tomita, K., Moossa, A. R., and Hoffman, R. M. (2003a). Determination of clonality of metastasis by cell-specific color-coded fluorescent-protein imaging. *Cancer Res.* **63**, 7785–7790.
- Yamamoto, N., Yang, M., Jiang, P., Xu, M., Tsuchiya, H., Tomita, K., Moossa, A. R., and Hoffman, R. M. (2003b). Real-time imaging of individual fluorescent-protein color-coded metastatic colonies *in vivo*. *Clin. Exp. Metastasis* **20**, 633–638.
- Yamauchi, K., Yang, M., Jiang, P., Yamamoto, N., Xu, M., Amoh, Y., Tsuji, K., Bouvet, M., Tsuchiya, H., Tomita, K., Moossa, A. R., and Hoffman, R. M. (2005). Real-time *in vivo* dual-color imaging of intracapillary cancer cell and nucleus deformation and migration. *Cancer Res.* **65**, 4246–4252.
- Yang, M., Baranov, E., Jiang, P., Sun, F. X., Li, X. M., Li, L., Hasegawa, S., Bouvet, M., Al-Tuwaijri, M., Chishima, T., Shimada, H., Moossa, A. R., Penman, S., and Hoffman, R. M. (2000). Whole-body optical imaging of green fluorescent protein-expressing tumors and metastases. *Proc. Natl. Acad. Sci. USA* **97**, 1206–1211.
- Yang, M., Baranov, E., Li, X. M., Wang, J. W., Jiang, P., Li, L., Moossa, A. R., Penman, S., and Hoffman, R. M. (2001). Whole-body and intravital optical imaging of angiogenesis in orthotopically implanted tumors. *Proc. Natl. Acad. Sci. USA* **98**, 2616–2621.

- Yang, M., Baranov, E., Wang, J-W., Jiang, P., Wang, X., Sun, F. X., Bouvet, M., Moossa, A. R., Penman, S., and Hoffman, R. M. (2002). Direct external imaging of nascent cancer, tumor progression, angiogenesis, and metastasis on internal organs in the fluorescent orthotopic model. *Proc. Natl. Acad. Sci. USA* **99**, 3824–3829.
- Yang, M., Chishima, T., Wang, X., Baranov, E., Shimada, H., Moossa, A. R., and Hoffman, R. M. (1999b). Multi-organ metastatic capability of Chinese ovary cells revealed by green fluorescent protein (GFP) expression. *Clin. Exp. Metastasis* **17**, 417–422.
- Yang, M., Hasegawa, S., Jiang, P., Wang, X., Tan, Y., Chishima, T., Shimada, H., Moossa, A. R., and Hoffman, R. M. (1998). Widespread skeletal metastatic potential of human lung cancer revealed by green fluorescent protein expression. *Cancer Res.* **58**, 4217–4221.
- Yang, M., Jiang, P., Sun, F. X., Hasegawa, S., Baranov, E., Chishima, T., Shimada, H., Moossa, A. R., and Hoffman, R. M. (1999a). A fluorescent orthotopic bone metastasis model of human prostate cancer. *Cancer Res.* **59**, 781–786.
- Yang, M., Li, L., Jiang, P., Moossa, A. R., Penman, S., and Hoffman, R. M. (2003). Dual-color fluorescence imaging distinguishes tumor cells from induced host angiogenic vessels and stromal cells. *Proc. Natl. Acad. Sci. USA* **100**, 14259–14262.
- Yang, M., Reynoso, J., Jiang, P., Li, L., Moossa, A. R., and Hoffman, R. M. (2004). Transgenic nude mouse with ubiquitous green fluorescent protein expression as a host for human tumors. *Cancer Res.* **64**, 8651–8656.
- Zolotukhin, S., Potter, M., Hauswirth, W. W., Guy, J., and Muzyczka, N. (1996). A 'humanized' green fluorescent protein cDNA adapted for high-level expression in mammalian cells. *J. Virol.* **70**, 4646–4654.

Further Reading

- Hoffman, R. M. (2002). Green fluorescent protein imaging of tumour growth, metastasis, and angiogenesis in mouse models. *Lancet Oncology* **3**, 546–556.
- MacDonald, T. J., Tabrizi, P., Shimada, H., Zlokovic, B. V., and Laug, W. E. (1998). Detection of brain tumor invasion and micrometastasis *in vivo* by expression of enhanced green fluorescent protein. *Neurosurgery* **43**, 1437–1442.
- Shaner, N. C., Campbell, R. E., Steinbach, P. A., Giepmans, B. N., Palmer, A. E., and Tsien, R. Y. (2004). Improved monomeric red, orange, and yellow fluorescent proteins derived from *Discosoma* sp. red fluorescent protein. *Nat. Biotechnol.* **22**, 1567–1572.



Chapter 6, Figure 1 Extravasation of tumor cells from vessels containing numerous dual-color HT1080 fibrosarcoma cells in a living mouse. HT1080 human fibrosarcoma cells were labeled with histone-H2B-GFP in the nucleus and with retroviral RFP in the cytoplasm. Cells were injected in the heart and visualized in skin vessels by whole-body imaging. From K. Yamauchi and R. M. Hoffman, unpublished data.